An Array Feed Radial Basis Function Tracking System for NASA's Deep Space Network Antennas

R. Mukai, P. Arabshahi, V.A.Vilnrotter

Jet Propulsion Laboratory
California Institute of Technology
4800 Oak Grove Dr., MS 238-343
Pasadena, CA 91109–8099 USA
{mukai, payman, vic}@dsp.jpl.nasa.gov

Abstract: *The use of radial basis function networks for fine pointing NASA's 70-meter deep space network antennas is described and evaluated. We demonstrate that such a network, working in conjunction with the array feed compensation system, and trained using the computationally efficient orthogonal least-squares algorithm, can point a 70-meter deep space antenna with rms errors of less than 0.3 millidegree under good signal-to-noise ratio conditions, achieving significantly higher accuracies than the 0.8 millidegree benchmark for communications at Ka-band frequencies of 32 GHz.*

1 Problem Statement

The NASA Deep Space Network – or DSN – is an international network of steerable, high-gain reflector antennas, which supports interplanetary spacecraft missions, radio and radar astronomy observations for the exploration of the solar system and the universe, and select Earth-orbiting missions. The DSN currently consists of three deep-space communication facilities, placed approximately 120° apart around the world, at Goldstone, in California's Mojave Desert; near Madrid, Spain; and near Canberra, Australia. This strategic placement permits constant observation of spacecraft as the Earth rotates, and helps make the DSN the largest and most sensitive scientific telecommunications system in the world.[1]

Over the past years, there has been increasing interest in the use of shorter carrier wavelengths to enhance the DSN's telecommunications and radio science capabilities. Shorter carrier wavelengths, or equivalently higher carrier frequencies, yield greater antenna gains and increased useful bandwidth, with reduced sensitivity to deep-space plasma effects, which tend to degrade the quality of the received signal. However, there are also new problems associated with the use of higher carrier frequencies, namely greater losses due to gravity-induced antenna deformations and wind, greater sensitivity to misalignments of the radio-frequency (RF) components, and more stringent pointing requirements – all of which are further complicated by time-varying distortions imposed on the antenna structure.

As the antenna tracks the target source (whether it is a spacecraft or a radio-source), time and elevation dependent loss components are introduced due to the Earth's rotation and the relative motion of the spacecraft, even in the absence of external disturbances. The combination of these factors can lead to unacceptably large pointing errors and signal-to-noise-ratio (SNR) losses if left uncorrected. Fortunately, most of these losses can be recovered by means of a properly designed compensation and tracking system that extracts the relevant deformation and pointing information from the received signal in real-time.

A recently developed approach [1] for recovering losses due to gravitational deformations, thermal distortion and wind consists of a real-time compensation system employing an array of feeds in the focal plane of the antenna's subreflector. The potential benefits of array feed combining for recovering losses due to mechanical antenna distortions at high frequencies (32 GHz or higher) have been described in [2-4]. The seven-element focal-plane Array Feed Compensation System (AFCS) described in [1], was designed and constructed at JPL. It has been evaluated at the DSN's Goldstone complex, and has successfully demonstrated real-time gravity-compensation and closed-loop tracking of spacecraft and radio-source signals at Ka-band frequencies (nominally 32 GHz).

---

[1] For more details on the Deep Space Network, please consult JPL's Telecommunications and Mission Operations Directorate (TMOD) at http://deepspace.jpl.nasa.gov. This work was funded by the TMOD Technology Program, and performed at the Jet Propulsion Laboratory, California Institute of Technology, under contract with the National Aeronautics and Space Administration.

A conceptual block diagram of the Ka-band AFCS designed for the DSN's 70-meter antennas is shown in Fig. 1.1. Its main components are an array of seven 22 dBi horns with a separate Ka-band low-noise amplifier (LNA) connected to each horn; a seven-channel downconverter assembly that converts the 32 GHz RF signal to 300 MHz IF, followed by a seven-channel baseband downconverter assembly that generates 14 real (seven complex) baseband signals; and a bank of 14 analog-to-digital converters, followed by a digital signal processing assembly that extracts parameters from the digital samples in real-time to obtain the optimum combining weights and determine the antenna pointing updates needed to maximize the combined SNR.

In the absence of antenna distortions, a single properly designed receiving horn collects virtually all of the focused signal power. Distortions generally lead to a shift in the peak of the signal distribution, as well as an effective "defocusing" of the power distribution in the focal plane. This defocusing leads to loss of power in the central channel, which can nevertheless be recovered by the outer horns of the array: when multiplied by complex combining weights matched to the instantaneous magnitude and phase of the signal in each channel, the SNR of the combined channel can be improved, approaching that of an undistorted antenna under ideal conditions. Distortions also affect the pointing of the antenna by introducing shifts in the signal peak: our intent here is to demonstrate that a properly designed radial basis function (RBF) neural network effectively removes time-varying pointing offsets and keeps the antenna pointed in the desired direction even in the presence of *significant* antenna distortions and other disturbances.

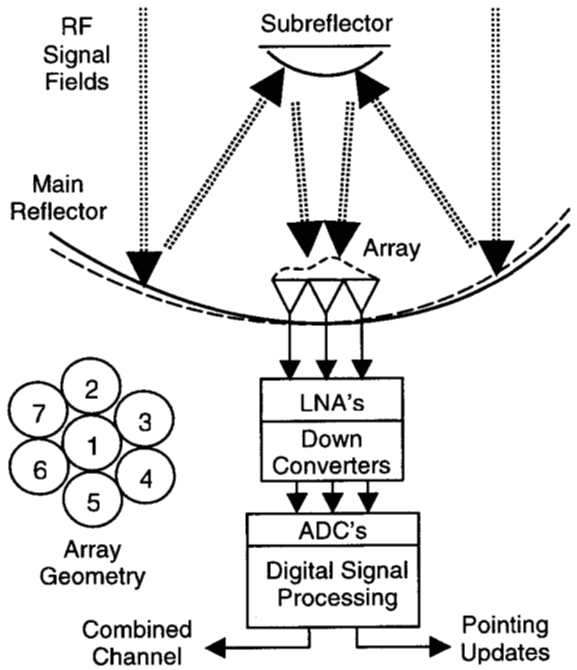

Figure 1.1: Conceptual Block Diagram of the Array Feed Compensation-tracking System.

2 Data Modeling and Preprocessing

When the antenna is pointed towards a source such as a distant spacecraft[2], here assumed to be transmitting a simple unmodulated carrier, the signal in the kth receiving channel can be represented as

$$r_k(t) = s_k(t) + n_k(t) \qquad k = 1, 2, \ldots, K \tag{2.1}$$

where K is the total number of channels (in this case K=7), and where the signal, $s_k(t)$, and background noise components, $n_k(t)$, are defined as

$$s_k(t) = \sqrt{2} S_k \cos(\omega t + \theta_k) \tag{2.2}$$

$$n_k(t) = \sqrt{2}[n_{ck}(t)\cos(\omega t) + n_{sk}(t)\sin(\omega t)] \tag{2.3}$$

[2] The signal source for generating the training and test data sets was the 32 GHz residual carrier of the DS1 spacecraft which was in cruise mode near Earth at the time, and thus provided a strong and stable signal.

Here $n_{ck}(t)$ and $n_{sk}(t)$ are uncorrelated baseband random processes representing the in-phase and quadrature components of the noise. Both the amplitude S_k and phase θ_k of the signal depend on the distortion of the antenna, and also on the pointing offset. After down conversion to in-phase and quadrature baseband, these waveforms are sampled, yielding the complex samples

$$r_k(i) = s_k(i) + n_k(i) \qquad k = 1, 2, \ldots, K \tag{2.4}$$

$$s_k(i) \equiv S_k e^{j\theta_k} \qquad E\, n_k(i) = 0 \qquad E|\, n_k(i)\,|^2 = \mathrm{var}[r_k(i)] = \sigma^2 \tag{2.5}$$

We assume that noise samples from different channels are independent, as are different noise samples in the same channel. It is convenient to represent the received samples as the K dimensional vectors $\mathbf{r}(i) = \mathbf{s}(i) + \mathbf{n}(i)$, where $\mathbf{r}(i) = (r_1(i), r_2(i), \ldots, r_K(i))$ and where each component is defined in Eqs. 2.4 and 2.5. In order to reduce the variance of the noise, the final training data consisted of averages of a large number of consecutive received vectors:

$$\mathbf{r}_a = \frac{1}{N}\sum_{i=1}^{N}\mathbf{r}(i) \qquad \text{where now } \mathrm{var}(\mathbf{r}_a) = \frac{\sigma^2}{N} \tag{2.4}$$

Prior to gathering the necessary training and test data, the antenna pointing needs to be refined. This is done while the signal's residual carrier is tracked, by means of a "five-point bore-sighting" algorithm. This technique introduces ±4 millidegree pointing offsets in two orthogonal directions along the line-of-sight (elevation *EL* and cross-elevation *XEL*); measures the signal power in the central horn (channel 1) at each offset, as well as with no offset (nominal on-source direction); and computes a pointing update based on a quadratic fit to the data. After a few iterations the magnitude of the updates approaches zero and the signal power in the central channel is maximized: this is considered to be the true "on-source" direction, and the antenna is then allowed to track the source using its own tracking model which takes into account both the rotation of the earth and the relative motion of the spacecraft.

Following this fine-pointing operation a raster-scan is initiated for data collection, whereby the antenna is commanded to predetermined offsets from the nominal on-source direction, and the received vector measured at each point. The raster-scan consists of the offsets 0, ±2, ±4, ±6 millidegrees in both the elevation and cross-elevation directions. Note that the zero-offset case defines the effect of antenna distortions on the received complex signals at that elevation, whereas the other cases contain a mixture of both distortion and pointing effects.

In order to remove possible time-dependent variations in the data, the data vectors were normalized by the complex value of the central horn (channel 1), so that the real and imaginary parts of the first component is always (1,0). Thus, only the response of the six outer horns was used to train the network.

Since the antenna distortion is elevation-dependent, training data from the raster scans was collected at virtually all elevations from less than 10° (near the horizon) to over 80° (close to zenith). The data was grouped in elevation bands spanning 0–10° elevation, 10–20°, and so on, up to the highest band covering 80–90°.

3 Training

During actual tracking, inaccuracies in the tracking model cause a slow drift away from the source, while wind gusts can introduce rapid pointing offsets of several millidegrees. Since Ka-band communications requires a pointing accuracy of 0.8 millidegrees or better to keep signal losses below 0.1 dB, it is necessary for the radial basis network to estimate the antenna pointing offset induced by these factors so that the antenna can be quickly pointed back on source. Using the complex numbers from the array feed, the networks can estimate the pointing offset in both *EL* and *XEL* with very high accuracy.

The RBF network was designed using the computationally efficient orthogonal least squares algorithm given in [5]. This algorithm uses the training data points as radial basis function centers. Gaussian radial basis functions were employed in the single hidden layer and a linear combiner with bias weights was used in the output layer. The optimum set of weights was obtained as the solution to a least squares fitting problem as outlined in [6].

Since the center horn voltage was always normalized to $1 + j0$, it was not necessary to present it to the network. The network's inputs therefore consisted of the gross antenna elevation in radians, and the real and imaginary components of the six normalized horn voltages of the outer horns, for an input vector of size 13. The network was trained to generate values for the elevation (*EL*), or cross-elevation (*XEL*) – the "offsets"– corresponding to the inputs. Two separate networks are used with *EL* and *XEL* as outputs.

The test data were collected following the raster scan procedure described above, on two different days, which are referred to as day 29 and day 38. Day 29's data display high SNR, mostly exceeding 30 dB–Hz. On the other hand, day 38's data were gathered at SNR values that never exceeded 28 dB–Hz. Consequently, as will be seen, the RBF network yielded significantly better performance on day 29 data than on day 38 data.

Day	Variable	Basis Units	Basis Width
38	*XEL*	153	0.60
38	*EL*	77	0.58
29	*XEL*	33	0.48
29	*EL*	23	0.68

Table 3.1: Number of hidden layer basis units, and corresponding basis widths of the RBF network as a function of day, elevation (*EL*), and cross-elevation (*XEL*). The radial basis function widths were selected by examining the distances among input vectors in the training set, and by experimentation.

From Table 3.1 we note that the best networks for day 38 (low SNR resulting in both poorer accuracy and greater difficulties in antenna tracking) were generally more complex than those for day 29 (high SNR). Notwithstanding, pointing errors even for low SNR data (day 38) were ordinarily less than 1 millidegree for SNR greater than 20 dB–Hz, as will be seen.

4 Results

Table 4.1 highlights the performance obtained with our two data sets.

Day/ Region	Gross Elevation (deg)	Gross Azimuth (deg)	e_{XEL} (mdeg)	s_{XEL} (mdeg)	e_{XEL} (mdeg)	s_{XEL} (mdeg)	SNR (dB-Hz)	Direction of Gross *EL*
29/1	57.4-64.7	96.9-104.7	-0.0505	0.4207	0.0507	0.4147	30 to 40	Rising
29/1	57.4-64.7	96.9-104.7	0.1501	0.3152	-0.0204	0.2708	> 40	Rising
29/3	61.1-65.0	254.4-259.1	0.1318	0.4112	0.0419	0.4153	30 to 40	Falling
29/4	55.1-59.9	260.4-264.8	0.1262	0.6722	-0.1662	0.5116	30 to 40	Falling
29/4	55.1-59.9	260.4-264.8	0.2267	0.3488	-0.1797	0.3249	> 40	Falling
38/1	69.3-72.7	113.8-122.0	-0.1985	0.7383	0.0454	0.9468	20 to 30	Rising
38/4	77.3-79.6	142.0-191.9	-0.2711	0.6834	0.2703	0.6941	20 to 30	Rising
38/4	77.3-79.6	142.0-191.9	-1.1917	1.4167	-0.2350	1.1166	10 to 20	Rising

Table 4.1: Mean elevation & cross-elevation error (e_{XEL}, e_{EL}); corresponding standard deviations (s_{XEL}, s_{EL}), for test data on different regions of days 29 and 38; and corresponding gross elevation/azimuth, and SNR.

Performance is seen to be a strong function of SNR. For very low SNR, mean errors and error standard deviations can exceed 1 millidegree. For high SNR cases, errors are generally less than 0.5 millidegree, which exceeds the pointing accuracy requirement for Ka-band communications on the 70-meter deep space antenna.

Figures 4.1 and 4.2 illustrate the ability of the neural network to estimate the pointing offsets applied to the antenna. The light, thick lines indicate the amount by which the antenna was pointing away from the source either in the *EL* or in the *XEL* direction. The thin, dark lines indicate the radial basis network's estimate of this pointing offset. The error in estimating the antenna pointing offset is the vertical distance between the light, thick line and the thin, dark line. It can be seen that these lines are very close, highlighting the radial basis network's ability to estimate these pointing offsets very accurately.

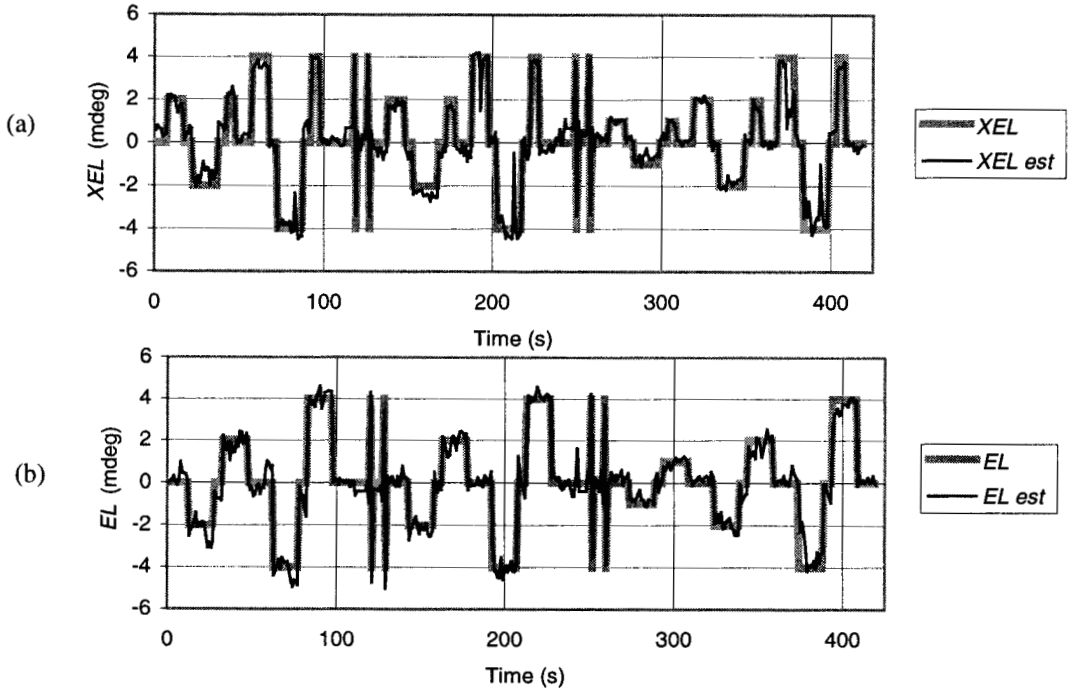

Figure 4.1: Day 29 *XEL* (a), and *EL* (b), Region 1 data.

Additional observations can be made from the two plots in Fig. 4.1. First, the tracking is very close with errors generally well under 1 millidegree. We note that the noisy output of the radial basis network could be smoothed by averaging, thus achieving even better performance when tracking near the center. Such averaging was not performed here due to rapid changes in offset, especially at the ±4 millidegree spikes. In a practical situation, where the objective is to keep the antenna centered on source, we can take advantage of averaging to improve accuracy.

We note error spikes at the centers of the broader peaks and troughs in the true offset. These spikes are sometimes generated by changes in the "other" variable. For example, the mild dip in the radial basis network's estimate of *EL* just after 50 seconds in Fig. 4.2(b) is caused by a change in *XEL* occurring at the same point, resulting in some cross-coupling between *XEL* and *EL*, likely due to a slight misalignment of the array with respect to the antenna axes. Much sharper spikes are evident in *XEL* tracking between 150 and 200 seconds (Fig. 4.2(a)), caused by transitions in corresponding *EL* data (Fig. 4.2(b)). In a tracking situation, where the antenna is being kept on source by the radial basis network, it is unlikely that the coupling effect will be noticeable, since only small offsets are applied in each direction. Despite the errors resulting from coupling, the measured error standard deviations remain under 0.5 millidegree in both *XEL* and *EL*.

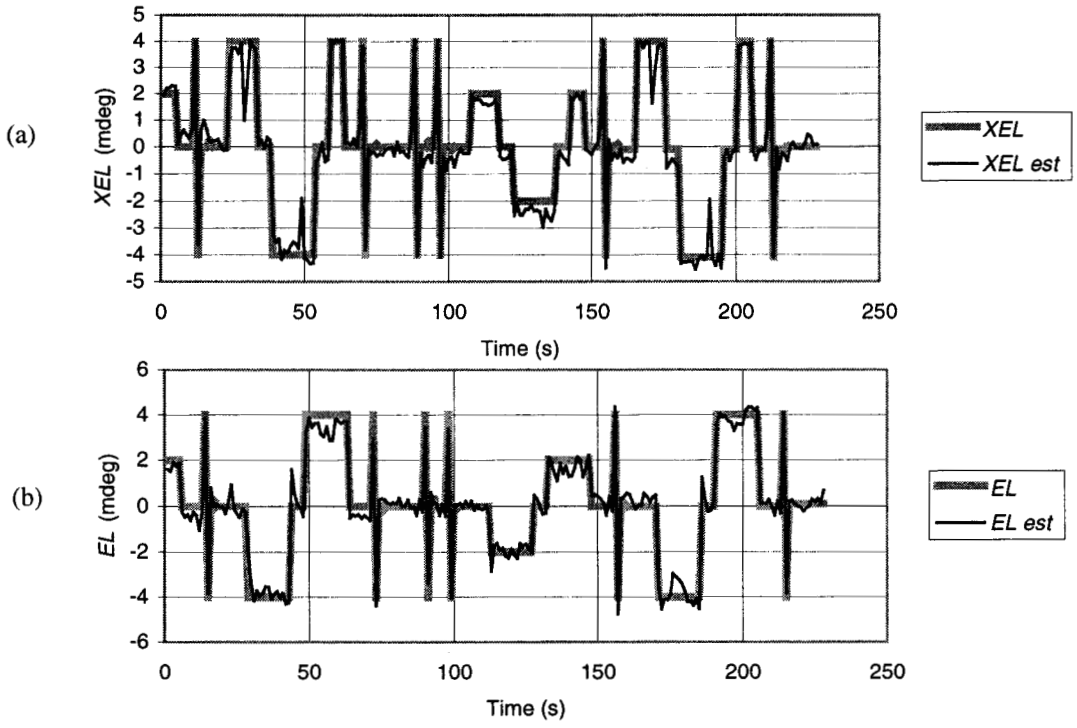

Figure 4.2: Day 29 *XEL* (a), and *EL* (b), Region 3 data.

5 Conclusions

Radial basis networks exhibit significant potential for keeping 70-meter deep space antennas pointed accurately on source. Using actual data gathered from such an antenna, it was possible to demonstrate that a radial basis network can track a source with errors less than 1 millidegree, and as good as 0.3 millidegree for a wide range of SNR values.

Future directions include adding power measurement to the tracking system to enable the radial basis network's linear combining weights in the output layers to be adapted to changes in the antenna. Age, seismic activity, and other factors may cause such changes.

References

[1] V.A. Vilnrotter, "Channel assignments for improved gain in baseband array feed compensation systems," *IEEE Trans. Communications,* vol. 42, pp. 2127–2133, May 1994.

[2] V.A. Vilnrotter, E.R. Rodemich, and S.J. Dolinar Jr., "Real-time combining of residual carrier array signals using ML weight estimates," *IEEE Trans. Communications*, vol. 40, pp. 604–615, March 1992.

[3] A.R. Cherrete, R.J. Acosta, P.T. Lam, and S.W. Lee, "Compensation of reflector antenna surface distortion using an array feed," *IEEE Trans. Antennas & Propagation*, vol. 37, pp. 966–978, August 1989.

[4] A.W. Rudge and D.E.N. Davies, "Electronically controllable primary feed for profile-error compensation of large parabolic reflectors," *Proc. IEEE*, vol. 117, pp. 351-358, February 1970.

[5] S. Chen, C.F.N. Cowan, and P.M. Grant, "Orthogonal Least Squares Learning Algorithm for Radial Basis Function Networks," *IEEE Trans. Neural Networks*, vol. 2, pp. 302–309, March 1991.

[6] S. Haykin, *Neural Networks: A Comprehensive Foundation*, New York: Macmillan, 1994, pp. 256–268.